Comparison of Classical and Fractional Viscoelastic Models for Describing Entangled Polymer Solutions

Robert Franz Schmidt[a)], *Horst Henning Winter*[b)], *Michael Gradzielski*[a),*]

[a)] *Stranski-Laboratorium für Physikalische und Theoretische Chemie, Institut für Chemie, Technische Universität Berlin, 10623 Berlin, Germany*

[b)] *Chemical Engineering and Polymer Science & Engineering, University of Massachusetts Amherst, Silvio O. Conte National Center for Polymer Research, 120 Governors Drive, Amherst, MA 01003-3110, USA*

For Table of Contents use only

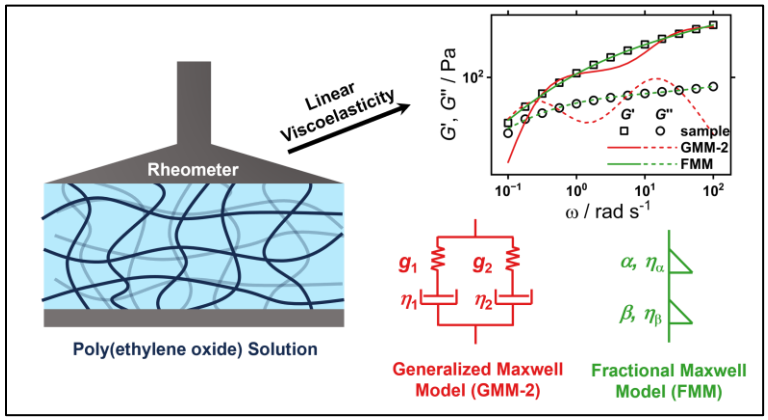

Abstract

Fractional viscoelastic models provide an excellent description of rheological data for polymer systems with power-law behavior. However, the physical interpretation of their model parameters, which carry fractional units of time, remains elusive. We show that for poly(ethylene oxide) (PEO) solutions, the fractional Maxwell model (FMM) requires fewer model elements than classical spring-dashpot models for a reasonable description of the data and that it can be applied consistently to solutions with varying degrees of viscoelasticity. The fractional parameters exhibit scaling laws similar to classical parameters as a function of polymer concentration. To attach physical meaning to the fractional parameters, we derive an analytical expression for the relaxation time spectrum associated with the FMM and find it to be equivalent to the empirical dual asymptote model.

Keywords

hydrogel, rheology, viscoelastic models, relaxation time spectrum, fractional model

1. Introduction

Many practically applied materials such as polymer solutions, food products, or biological tissues show viscoelastic behavior, meaning they exhibit both viscous and elastic properties, depending on the time frame of observation. Common rheological tests to determine the viscoelastic properties of a material include relaxation tests and oscillatory tests. In a relaxation test, the material is subjected to a step of strain γ_0, and the resulting time evolution of stress $\sigma(t)$ is recorded. The property $G(t) = \sigma(t)/\gamma_0$ is known as the relaxation modulus. In an oscillatory shear test, the sample is subjected to an oscillating shear strain $\gamma(\omega)$ as a function of oscillation frequency ω, and the resulting oscillating shear stress $\sigma(\omega)$ is recorded. The property $G^*(\omega) = G'(\omega) + iG''(\omega) = \sigma(\omega)/\gamma(\omega)$, is the complex modulus, where the real part G' (storage modulus) characterizes the elastic properties, and the imaginary part G'' (loss modulus) characterizes the viscous properties. To obtain a better understanding of a material's viscoelastic properties, mathematical models based on characteristic parameters are used to describe the viscoelastic behavior. Fitting mathematical models to experimental data allows the extraction of these model parameters, which can be related to microstructural relaxation processes. The obtained parameters can then easily be compared across samples to identify differences and/or similarities. Classical viscoelastic models comprise arrangements of elastic springs and viscous dashpots.[1] The resulting constitutive equations can be solved to yield a mathematical prediction of the material's response under various conditions. They generally produce an exponential behavior for the relaxation modulus with discrete relaxation times.

Real materials often exhibit a finite time window with distinctive power-law behavior in relaxation and oscillation tests. It occurs in materials with a broad range of relevant microstructural length and time scales.[2,3] In many cases, a quantitative link was found between the power-law exponent from rheological measurements and microscopic structure.[3–7] One example is Rouse motion in polymer physics, where the power-law rheology is an expression of the self-similarity of microscopic dynamics, which stems from the fractal structure.[3,8] Here, the fractal dimension, $d_f = 2$, is directly connected to the rheological power-law exponent of 0.5. Examples of real materials exhibiting power-law rheology include cells,[9,10] tissue,[11] biopolymer networks,[12] gluten gels,[13] or food products.[14]

A single power-law relaxation process, when discretized, expresses itself as a set of relaxation times and strengths, τ_i and g_i, which are equally spaced on a straight trajectory as plotted on log-log scale. More complicated is the interaction of two or more power-laws. Modeling such power-law behavior with traditional spring-dashpot models is an ill-posed problem, especially when using a very large number of spring-dashpots.[15–17] Instead, empirical mathematical models can be fitted to the data, but their parameters may lack physical meaning since they are not derived from constitutive equations. A third, more recent approach is provided by fractional calculus, a branch of mathematics that extends the concept of differentiation to non-integer

orders.[18] Introducing fractional derivative operators into rheological constitutive equations automatically leads to power-law predictions for material functions such as the relaxation modulus or the complex modulus.[19] Fractional viscoelastic models have been demonstrated to accurately describe a wide range of real materials, including Xanthan gum,[20,21] starch gels,[22] starch/polypropylene blends,[23] various liquid foods,[24] and polyacrylamide gels.[25] Using fractional models can greatly reduce the number of parameters needed for an accurate description of the data.[26–31] The review article by Bonfanti *et al.* [2] provides a good overview of various fractional viscoelastic models and their applications. One drawback of fractional viscoelastic models is that they introduce model parameters with units of fractional order in time. These model parameters, sometimes referred to as *quasi-properties*, lack direct physical meaning, but have been associated with the firmness of a material.[2,32–34] Depending on the fractional exponent, a quasi-property lies somewhere between a modulus with units of Pa and a viscosity with units of Pa s. In the present study, we demonstrate the advantages of using a fractional Maxwell model (FMM) over the classical generalized Maxwell model (GMM) for describing aqueous solutions of high molecular weight (M_w) poly(ethylene oxide) (PEO), which exhibit viscoelastic properties due to polymer chain entanglements.[35–38] We further determine how the FMM parameters scale as a function of polymer concentration. To elucidate the physical meaning of the quasi-properties, we derive an analytical expression for the relaxation time spectrum associated with the FMM.

2. Viscoelastic Models

Rheological behavior is usually described through constitutive equations, i.e., relationships between stress σ and strain γ. Classical viscoelastic models are composed of series-parallel arrangements of springs and dashpots, which are characterized by their modulus g and viscosity η, respectively. The constitutive equations for a viscous dashpot and an elastic spring are shown in Figure 1 A) and contain the first time derivative of strain and the "zero" time derivative of strain, respectively.

2.1 The generalized Maxwell model

One of the simplest viscoelastic models is the Maxwell model, which corresponds to a spring and a dashpot connected in series. It predicts an exponential decay of the relaxation modulus $G(t)$ with a characteristic relaxation time τ. In the generalized Maxwell model (GMM), also known as the Wiechert model, N Maxwell elements are connected in parallel, leading to a spectrum of discrete relaxation times.[1,39] A schematic representation of the GMM is shown in Figure 1 B).

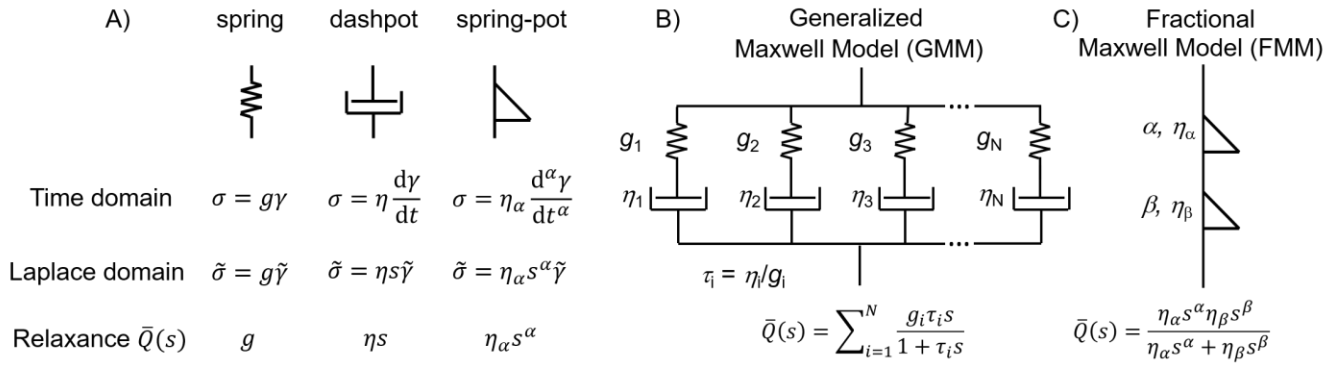

Figure 1: Sketches of A) the spring, dashpot and spring-pot model elements and their constitutive equations, B) the generalized Maxwell model, and C) the fractional Maxwell model.

The relaxation modulus and storage/loss moduli of the GMM with *N* modes are given by

$$G(t) = \sum_{i=1}^{N} g_i \exp\left(-\frac{t}{\tau_i}\right) \tag{1}$$

and

$$G'(\omega) = \sum_{i=1}^{N} g_i \frac{\omega^2 \tau_i^2}{1 + \omega^2 \tau_i^2} \tag{2}$$

$$G''(\omega) = \sum_{i=1}^{N} g_i \frac{\omega \tau_i}{1 + \omega^2 \tau_i^2} \tag{3}$$

, where t_i and g_i are the relaxation time and strength of the *i*-th mode, respectively. The set of relaxation times and strengths is also known as the relaxation time spectrum $H(\tau)$ of a material, which can be a continuous function or a sum of discreet terms.[17,40,41] $H(\tau)$ is the kernel of several rheological functions, including

$$G(t) = g_0 + \int_0^{\tau_{max}} H(\tau) \exp(-t/\tau) \frac{d\tau}{\tau} \tag{4}$$

$$G'(\omega) = g_0 + \int_0^{\tau_{max}} H(\tau) \frac{\omega^2 \tau^2}{1 + \omega^2 \tau^2} \frac{d\tau}{\tau} \tag{5}$$

$$G''(\omega) = \int_0^{\tau_{max}} H(\tau) \frac{\omega\tau}{1+\omega^2\tau^2} \frac{d\tau}{\tau} \quad (6)$$

where τ_{max} is the longest relaxation time and g_0 is the equilibrium modulus, which is 0 for liquids and > 0 for solids. Knowledge of $H(\tau)$ thus allows to calculate those material functions. However, calculating $H(\tau)$ from G' and G'' is a mathematically ill-posed problem. There have been numerous publications in the past concerning approaches to determining $H(\tau)$ from oscillatory shear data.[17,42–52] These approaches differ in terms of the employed algorithms, and all have strengths and weaknesses.[42] One particular example is the parsimonious modeling approach, where an unbiased fit function is used for $H(\tau)$ that describes the data with the least possible number of relaxation modes.[17] The discrete relaxation times can then be converted into a continuous spectrum.[40] Other examples for algorithms include using a nonlinear-regularization method to overcome the problems of Tikhonov regularization,[53] or cubic Hermite splines.[52] It should be noted that in principle there is an infinite number of discrete spectra that describe the data within experimental error.[51] Baumgaertel and Winter analyzed the mathematical problem of fitting discrete modes to dynamic mechanical data and realized that an intermediate number of modes, N, significantly reduces ill-posedness, as shown with several examples.[40] In this approach, ill-posedness no longer poses a problem and, as an example, allows to reliably deduce the relaxation spectrum for long linear flexible polymers.[54]

Another possibility to overcome the ill-posedness of eqns (4)-(6) is to set $H(\tau)$ to be of a meaningful functional form, such as a Gaussian distribution or a log-normal distribution.[55,56] The distribution parameters, such as mean relaxation time or standard deviation can then be determined by nonlinear curve-fitting of eqns (4)-(6). However, this method is only useful in cases, where the expected functional form of $H(\tau)$ is already known.

2.2 The fractional Maxwell model

Fractional viscoelasticity refers to a class of models that incorporate fractional derivates in their constitutive equations. The corresponding model element is known as a spring-pot (sometimes also Scott-Blair element) referencing its ability to interpolate between a spring and a dashpot.[57,58] Its constitutive equation is given by

$$\sigma(t) = \eta_\alpha \frac{d^\alpha}{dt^\alpha} \gamma(t) \quad (7)$$

where d^α/dt^α is the Caputo fractional derivative,[59] $0 \leq \alpha \leq 1$ is the fractional exponent and η_α is a quasi-property, descriptive of the magnitude of the spring-pot's resistance against deformation.[32,60] The spring-pot degenerates into a spring for $\alpha = 0$ and into a dashpot for $\alpha = 1$. Conversion of equation (7) into the Laplace domain yields a factor of s^α, which explains why fractional

viscoelastic models exhibit power-law behavior in the frequency domain. Spring-pots can be combined with classical springs and dashpots as well as with other spring-pots to form viscoelastic models that can describe complex rheological behavior with a minimal number of parameters. One particular example is the fractional Maxwell model (FMM), which, in analogy to the classical Maxwell model, connects two spring-pots in series. A schematic representation of the FMM is shown in Figure 1. The FMM is governed by two fractional exponents, $0 \leq \beta < \alpha \leq 1$. The more elastic spring-pot with the lower exponent β determines the short-time/high-frequency behavior, $G(t \to 0) \sim t^{-\beta}$, $G'(\omega \to \infty) \sim \omega^{\beta}$ and the more viscous spring-pot with the higher exponent α determines the long-time/low-frequency behavior, $G(t \to \infty) \sim t^{-\alpha}$, $G'(\omega \to 0) \sim \omega^{\alpha}$.[2] For $\beta = 0$ and $\alpha = 1$, the regular Maxwell model is retrieved. The storage and loss moduli are given by:[2]

$$G'(\omega) = \frac{\left(\eta_\beta \omega^\beta\right)^2 \cdot \eta_\alpha \omega^\alpha \cos(\alpha\pi/2) + (\eta_\alpha \omega^\alpha)^2 \cdot \eta_\beta \omega^\beta \cos(\beta\pi/2)}{(\eta_\alpha \omega^\alpha)^2 + \left(\eta_\beta \omega^\beta\right)^2 + 2\eta_\alpha \omega^\alpha \cdot \eta_\beta \omega^\beta \cos((\alpha-\beta)\pi/2)} \tag{8}$$

$$G''(\omega) = \frac{\left(\eta_\beta \omega^\beta\right)^2 \cdot \eta_\alpha \omega^\alpha \sin(\alpha\pi/2) + (\eta_\alpha \omega^\alpha)^2 \cdot \eta_\beta \omega^\beta \sin(\beta\pi/2)}{(\eta_\alpha \omega^\alpha)^2 + \left(\eta_\beta \omega^\beta\right)^2 + 2\eta_\alpha \omega^\alpha \cdot \eta_\beta \omega^\beta \cos((\alpha-\beta)\pi/2)} \tag{9}$$

The FMM has been successfully applied to describe the rheological behavior of rock,[61] sandstone,[62] colloidal gels,[3] atrial tissue,[63] food gels,[14] or collagen gel,[64] to name a few.

3. Materials and Methods

3.1 Sample Preparation

Aqueous semi-dilute solutions of high-M_w poly(ethylene oxide) (PEO) were prepared gravimetrically by adding the appropriate masses of PEO to a 4 mL glass vial. PEO with average molecular weights M_w of 1000, 2000 and 4000 kDa were used, each obtained from Sigma-Aldrich. Milli-Q water containing 0.003 %w/v polystyrene particles (~200 nm diameter) was then added using an Eppendorf pipette to obtain the desired final polymer weight percentage c. The polystyrene particles were originally added to allow for dynamic light scattering microrheology experiments, as shown in ref [65]. They do not interfere with the macroscopic oscillatory rheology experiments and will therefore not be considered any further. The samples were stirred using a magnetic stirrer until a homogeneous solution was obtained, which required up to 1-2 days depending on c and M_w.

3.2 Rheology

Oscillatory shear experiments were performed on an MCR 502 WESP temperature-controlled rheometer from Anton Paar (Graz, Austria) in strain-imposed mode using a cone and plate measuring system with a 50 mm diameter and a cone angle of

1°. The gap width was fixed at 101 µm. The temperature was kept fixed at 25 °C for all measurements. In two successive frequency sweeps, the oscillation frequency was varied between 0.1 and 100 rad/s first in increasing and then decreasing order to check for hysteresis effects. Since no significant differences between both sweeps were found, only the first of the two sweeps was considered further. The strain amplitude was kept fixed at 5%. This value lies well within the linear viscoelastic regime, as demonstrated by amplitude sweeps that can be found in the supporting material (see Figure S1).

3.3 Fitting viscoelastic models

Viscoelastic models were fitted using the lmfit package in Python, which utilizes a non-linear least-squares optimization routine.[66] Model functions were written to return a one-dimensional array containing G' and G'', so both the real and the imaginary parts are fitted at the same time. The minimized quantity is given by:

$$\chi^2 = \sum_{i=1}^{N} \left(\frac{G_i'^{\text{data}} - G_i'^{\text{model}}}{G_i'^{\text{data}}} \right)^2 + \left(\frac{G_i''^{\text{data}} - G_i''^{\text{model}}}{G_i''^{\text{data}}} \right)^2 \tag{10}$$

where dividing by $G_i'^{\text{data}}$ and $G_i''^{\text{data}}$ ensures that all data points are considered equally.

4. Results

4.1 Fit quality of classical vs fractional models

As an example, frequency sweeps performed on a 3 wt% solution of 4000 kDa poly(ethylene oxide) (PEO) shall be discussed here in detail. The G', G'' data were fitted with the generalized Maxwell model GMM-N with an increasing number of modes, $N = 1 \ldots 4$, as well as with fractional Maxwell model, FMM. In addition, the parsimonious spectrum was determined using the IRIS rheology software.[67,68] The fits are shown in Figure 2 A) together with the residuals in B).

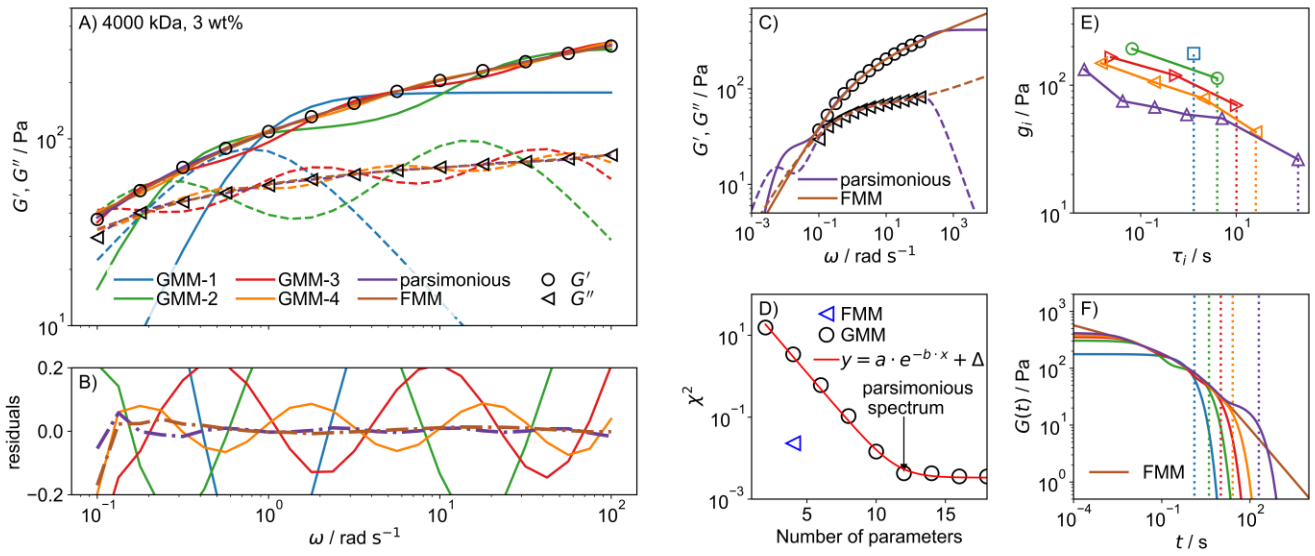

Figure 2: A) Fits of GMM-*N* with increasing number of modes $N = 1$ to $N = 4$, the parsimonious model and the FMM for a 4000 kDa, 3 wt% PEO solution. Only every second data point is shown to improve lucidity. Solid and broken lines indicate *G*' and *G*'', respectively. B) Relative fit residuals (data – model) / data. The parsimonious model and FMM are shown with dashdot lines. C) The fit parameters of the parsimonious and FMM models are used to predict *G*' and *G*'' outside of the data range. D) The fit error χ^2 as a function of the number of model parameters. E) Relaxation time spectra determined from GMM fits with an increasing number of modes. F) Predictions for the relaxation modulus calculated using equation (1) for GMM and using the Mittag-Leffler function for the FMM. The dotted lines indicate the longest relaxation time of each spectrum. The color code in E) and F) is the same as in A).

The number of model parameters is $2N$ for GMM-*N*, 4 for FMM and, in this particular case, 12 for the parsimonious model. When a small number of modes is used, the GMM, which predicts $G' \sim \omega^2$ and $G'' \sim \omega$ scaling for $\omega \to 0$, struggles to reproduce the weak frequency dependence of *G*' and *G*'' seen in the data. The fit curves oscillate about the data and at least four modes are necessary for a reasonable description of the data. The parsimonious model yields a very good description with $N = 6$ modes. In comparison, the FMM achieves an excellent description over the whole frequency range with only 4 parameters. One marked difference between the two types of models becomes clear when the fitted functions are extended to frequencies below and above the measured (and fitted) range, as shown in Figure 2 C). The parsimonious model predicts a second crossover of *G*' and *G*'' at low frequencies, for which there is no evidence based on the data. This indicates that the determined discrete modes are only valid in the fitted range and therefore constitute only a fraction of the whole material response. The prediction of the FMM

outside the fit range is smoother and looks much more realistic. The four model parameters of the FMM thus capture the rheology of the sample even outside the measured time range.

To quantify the fit quality, the chi-square statistic χ^2, equation (10), is shown in Figure 2 D) as a function of the number of model parameters. For the GMM-type models, χ^2 decreases exponentially with the number of model parameters until a limiting value, Δ, is reached, which can be associated with the noise level of the data.[40] The spectrum with the lowest number of model parameters that reaches a fit error close to Δ is known as the parsimonious spectrum. The FMM reaches a fit error lower than GMM-4 with half the number of fit parameters.

4.2 Implications for the time domain

The relaxation times τ_i and strengths g_i of the GMM fits with increasing number of modes are shown in Figure 2 E) and F). The relaxation time spectrum widens as the number of modes is increased until it spans from around 10^{-2} s to 10^2 s, which corresponds to the inverse of the measured frequency range. This corroborates the earlier statement that the determined spectrum merely reflects the time scale of the experiment. If fewer Maxwell modes are fitted, the individual relaxation strengths g_i are stronger to compensate. We can thus presume that a continuous relaxation time spectrum $H(\tau)$ should always have lower values than any discrete spectrum.

To compare the behavior of the models in the time domain, we can use equation (1) to predict the relaxation modulus for the GMM. For the FMM, the relaxation modulus is given by:[2]

$$G(t) = \eta_\beta t^{-\beta} E_{\alpha-\beta,1-\beta}\left(-\frac{\eta_\beta}{\eta_\alpha} t^{\alpha-\beta}\right) \tag{11}$$

where $E_{a,b}(z)$ is the two-parameter Mittag-Leffler function (MLF). The MLF, which is capable of interpolating between exponential and power-law behavior, appears frequently in fractional calculus and is given by

$$E_{a,b}(z) = \sum_{k=0}^{\infty} \frac{z^k}{\Gamma(b+ak)}, \quad a > 0, \qquad b \in \mathbb{R}, z \in \mathbb{C} \tag{12}$$

More details about the MLF and its limiting behavior can be found in refs [69–71]. In this paper, the MLF was evaluated numerically in MATLAB.[72,73] The $G(t)$ predictions of the GMM and FMM are similar in the intermediate time range that corresponds to the measured frequency range. Differences arise in the limiting behavior. The GMM quickly approaches a

constant plateau value for times t shorter than the shortest relaxation time. The plateau is given by the sum of all relaxation strengths, $G(t \to 0) = \sum_{i=0}^{N} g_i$. At times longer than the longest relaxation time (demonstrated by the dotted lines in Figure 2 E) and F)), $G(t)$ decays exponentially. The FMM on the other hand predicts power-law behavior in both limits, specifically $G(t \to 0) \sim \eta_\beta t^{-\beta}$ and $G(t \to \infty) \sim (1\text{-}\alpha)\eta_\alpha t^{-\alpha}$. Accordingly, the FMM is typically the much more realistic description, as it is less bound to reflect the artefacts seen in the GMM arising from the limited experimental window and the intrinsically assumed exponential relaxation.

The terminal power-law behavior of the FMM has implications for the zero-shear viscosity η_0, which is fully defined by the relaxation modulus [74]

$$\eta_0 = \int_0^\infty \mathrm{d}t\, G(t) \tag{13}$$

For this discussion, the relaxation modulus of the FMM may be approximated by two power-laws (neglecting the transition from one to the other)

$$G(t) = \begin{cases} G_{\mathrm{FMM}} t^{-\beta} \text{ for } t < \tau_{\mathrm{FMM}} \\ G_{\mathrm{FMM}} t^{-\alpha} \text{ for } t > \tau_{\mathrm{FMM}} \end{cases} \tag{14}$$

where $\tau_{FMM} = \left[(1-\alpha)\,\eta_\alpha/\eta_\beta\right]^{1/(\alpha-\beta)}$ is the time, where the two power-laws intersect and $G_{\mathrm{FMM}} = \eta_\beta\left[(1-\alpha)\,\eta_\alpha/\eta_\beta\right]^{\beta/(\beta-\alpha)}$ is the value of G at $t = \tau_{\mathrm{FMM}}$. A simple approximation as such can be used to explore the properties of the zero-shear viscosity of the FMM:

$$\eta_0 = \int_0^{\tau_{FMM}} \mathrm{d}t\, G(t) + \int_{\tau_{FMM}}^\infty \mathrm{d}t\, G(t) \tag{15}$$

, which rearranges into

$$\begin{aligned} \frac{\eta_0}{G_{\mathrm{FMM}}\tau_{\mathrm{FMM}}} &= \int_0^{\tau_{\mathrm{FMM}}} \frac{\mathrm{d}t}{\tau_{\mathrm{FMM}}}\left(\frac{t}{\tau_{\mathrm{FMM}}}\right)^{-\beta} + \int_{\tau_{\mathrm{FMM}}}^\infty \frac{\mathrm{d}t}{\tau_{\mathrm{FMM}}}\left(\frac{t}{\tau_{\mathrm{FMM}}}\right)^{-\alpha} \\ &= \frac{1}{1-\beta} + \frac{1}{1-\alpha}\lim_{(t/\tau_{FMM})\to\infty}\left(\frac{t}{\tau_{FMM}}\right)^{1-\alpha} - 1 = \lim_{(t/\tau_{FMM})\to\infty}\left(\frac{t}{\tau_{FMM}}\right)^{1-\alpha} \end{aligned} \tag{16}$$

According to equation (16), the zero-shear viscosity of the FMM diverges. Such behavior is expected for materials at the gel point,[75–77] but not for solutions of non-crosslinked polymers.

While the predictions of the FMM are accurate over a wide time range, the power-law behavior must end at a finite time, corresponding to the longest slowest relaxation time, τ_{max}, to explain the presence of a finite zero-shear viscosity and the absence of a yield stress. That η_0 is indeed finite for the PEO solutions studied in this work is shown through steady-shear experiments in the supporting material (see Figure S4).

4.3 Relation between FMM parameters and the relaxation time spectrum $H(\tau)$

As shown in the previous section, the FMM successfully describes real materials. Presuming that any material is fully characterized by a relaxation time spectrum $H(\tau)$, we should be able to learn more about the spectrum that is associated with a FMM material. To explore this, we generated artificial data using the FMM for exemplary parameter values of $\alpha = 0.75$ and $\beta = 0.25$ as well as with varying values for η_α and η_β. The artificially created G' and G'' data was then analyzed using the IRIS software to determine the parsimonious spectra. The results are shown in Figure 3. The relaxation time spectra that were derived from the artificial FMM data consist of two power-law regions characterized by exponents α and β, that are the same as the FMM model parameters. The fastest and the slowest relaxation times, determined by IRIS, slightly deviate from the power-law prediction, most likely due to the finite frequency range of the generated data. If η_β is kept constant and η_α is varied (Figure 3 A) and C)), the fast power-law region, characterized by α, remains unchanged. The slow power-law region, characterized by α, is shifted upwards in y-direction with increasing η_α. The opposite is true if η_α is kept constant and η_β is increased (Figure 3 B) and D)). We can thus conclude that the relaxation time spectrum will be of the following functional form:

$$H_{FMM}(\tau) = \begin{cases} f_\beta(\beta, \eta_\beta)\tau^{-\beta} & \text{for } \tau < \tau_{\mathrm{FMM}}(\alpha, \eta_\alpha, \beta, \eta_\beta) \\ f_\alpha(\alpha, \eta_\beta)\tau^{-\alpha} & \text{for } \tau < \tau_{\mathrm{FMM}}(\alpha, \eta_\alpha, \beta, \eta_\beta) \end{cases} \quad (17)$$

where f_α and f_β are factors and τ_{FMM} is the intersection point between the two power-law regimes.

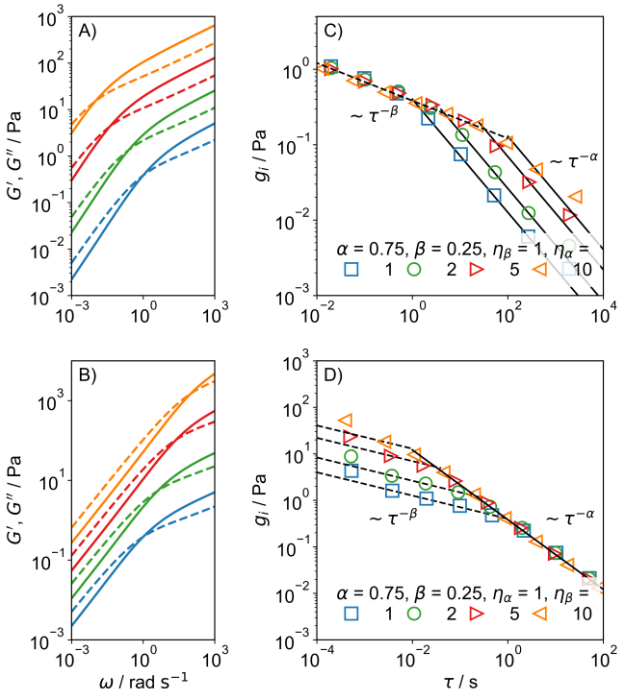

Figure 3: *G*' (full lines) and *G*'' (broken lines) data were artificially generated using the FMM for $\alpha = 0.75$ and $\beta = 0.25$ and A) constant η_β + increasing η_α, as well as B) constant η_α + increasing η_β. The color code in A) and B) is the same as in C) and D), respectively. η_α has units of Pa $s^{0.75}$ and η_β has units of Pa $s^{0.25}$. The *G*' and *G*'' data were then analyzed using the IRIS software to determine the parsimonious spectra, which are shown in C) and D). The spectra are characterized by two power-law regimes with exponents $-\alpha$ (full black lines) and $-\beta$ (dashed black lines).

To determine the factors f_α and f_β, we start by considering a simpler model, consisting of just one spring-pot. The relaxation modulus of a spring pot is given by[2]

$$G(t) = \frac{\eta_\alpha}{\Gamma(1-\alpha)} t^{-\alpha} \tag{18}$$

where $\Gamma(z)$ is the gamma function. The relaxation modulus and the relaxation time spectrum $H(\tau)$ are connected through equation (4). If we assume $H(\tau)$ to also be a power-law with the same exponent, we can write

$$\frac{\eta_\alpha}{\Gamma(1-\alpha)} t^{-\alpha} = f_\alpha \int_0^\infty \tau^{-\alpha} e^{-t/\tau} \frac{\mathrm{d}\tau}{\tau} \tag{19}$$

substituting with $u = t/\tau$ yields

$$\frac{\eta_\alpha}{\Gamma(1-\alpha)}t^{-\alpha} = f_\alpha t^{-\alpha}\int_0^\infty u^{\alpha-1}e^{-u}\mathrm{d}u \tag{20}$$

The integral is the gamma function $\Gamma(\alpha)$. Rearranging leads to an expression for f_α

$$f_\alpha = \frac{\eta_\alpha}{\Gamma(1-\alpha)\Gamma(\alpha)} \tag{21}$$

Assuming that both spring-pots in the FMM are independent, which is supported by the fact that the α-power-law region is unaffected by variation of η_β and vice versa, we can insert f_α and f_β into equation (17) to find an analytical expression for the relaxation time spectrum of the FMM:

$$H_{FMM}(\tau) = \begin{cases} \dfrac{\eta_\beta}{\Gamma(1-\beta)\Gamma(\beta)}\tau^{-\beta} & \text{for } \tau < \tau_{\mathrm{FMM}} \\ \dfrac{\eta_\alpha}{\Gamma(1-\alpha)\Gamma(\alpha)}\tau^{-\alpha} & \text{for } \tau < \tau_{\mathrm{FMM}} \end{cases} \tag{22}$$

where $\tau_{\mathrm{FMM}} = \left(\frac{\eta_\alpha}{\eta_\beta}\frac{\Gamma(1-\beta)\Gamma(\beta)}{\Gamma(1-\alpha)\Gamma(\alpha)}\right)^{\frac{1}{\alpha-\beta}}$.

Without reference to fractional viscoelasticity, expressions equivalent to eq. (22) have been used before to describe relaxation time spectra. An example is the 'dual asymptote model' or 'dual powerlaw model' by Winter and Mours,[67] which was chosen empirically to describe the spectra of sulfonic acid ionomer dispersions [78]. It is given by:

$$H_{\mathrm{d.a.}}(\tau) = H_i \frac{\left(\frac{\tau}{\tau_i}\right)^{-(n_l+n_u)}}{\left(\frac{\tau}{\tau_i}\right)^{-n_u} + \left(\frac{\tau}{\tau_i}\right)^{-n_l}} \tag{23}$$

, where H_i and τ_i are the values of $H_{\mathrm{d.a.}}$ and τ at the intersection point of the two power-laws and n_l and n_u are the two power-law exponents, equivalent to α and β, respectively.

To test equation (22), G' and G'' for two different sets of parameters α, β, η_α, η_β, were generated and their spectra determined through analysis by IRIS. The determined spectra as well as the corresponding predictions according to equation (22) are shown in Figure 4. Additionally, the spectra were fitted with the dual asymptote model, eq (23), the fit results are shown in Table 1.

Table 1: Results for the parameters of the dual asymptote model, that was fitted to artificially generated FMM data.

α	β	η_α / Pa s$^\alpha$	η_β / Pa s$^\beta$	n_l	n_u	H_i / Pa	τ_i / s
0.8	0.3	5	2	0.86 ± 0.07	0.29 ± 0.04	0.57 ± 0.35	7.44 ± 8.12
0.6	0.2	1	3	0.59 ± 0.04	0.16 ± 0.09	2.99 ± 2.29	0.05 ± 0.10

The prediction from the FMM model agrees well with the determined spectra, as well as with the dual asymptote model. The original exponents α and β are within the error ranges of n_u and n_l from the dual asymptote fit, verifying the equivalence of the two models. The values of H_{FMM} are slightly lower than those of the individual data points in the discrete spectra. As N increases and the total mechanical response is distributed across more modes, the relaxation strength of each individual mode decreases (see also Figure 2 E). It follows that the continuous, theoretical spectrum H_{FMM} with an infinite number of modes must always have lower values than those of any discrete spectrum. Equation (22) allows to make some more statements about the physical meaning of the fractional model parameters. In the GMM, each pair of spring and dashpot makes up one mode and contributes one point to the relaxation time spectrum. Each of those points is characterized by a relaxation strength g_i with units of Pa. If the strength of one mode g_j is increased, all remaining modes $i \neq j$ remain unchanged. In the FMM, each pair of fractional exponent + quasi-property corresponds to an infinite number of relaxation times in the form of a power-law. If η_α is increased, the whole group of relaxation modes is shifted to higher values.

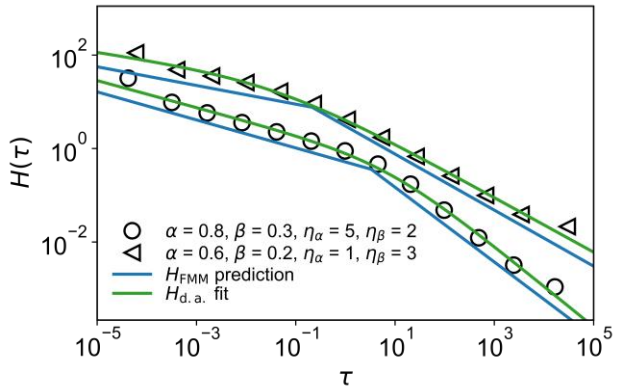

Figure 4: The spectra of artificially generated G' and G'' data for two different sets of FMM parameters were determined through fitting in IRIS, as well as through calculation according to equation (22). The spectra were also fitted with the dual asymptote model, equation (23).

4.4 Scaling of FMM parameters with concentration and molecular weight of PEO solutions

To obtain more insight about the FMM and its properties and apply it to a practical question of interest, it was fitted to a range of PEO solutions with varying molecular weight and concentration. The M_w of the PEO was varied from 1000 to 4000 kDa and the concentration from 1 to 4 wt%, which leads to rather low viscous solutions for the short PEO chains and low concentrations and hydrogel-like consistency for the high-M_w and high concentration, which is well known from previous investigations.[35–38] The change of the FMM parameters as a function of polymer concentration is shown in Figure 5. The quasi-properties η_α and η_β quantify the magnitude of the corresponding spring-pot's resistance against deformation and have units of Pa s^α and Pa s^β respectively. Each data point shown in Figure 5 A) belongs to a spring-pot with a different fractional exponent and therefore also carries a different physical unit. Interestingly, η_α and η_β still show a clear power-law dependence on concentration and thereby behave like regular physical properties. The scaling exponents n_α and n_β for η_α and η_β, respectively, are given in Table 2. The more viscosity-like quasi-property η_α, generally shows a stronger dependence on concentration than the more modulus-like property η_β. This is in agreement with the predicted behavior for entangled polymer systems for which one expects a power-law with an exponent 2.0-2.3 for the concentration dependence of the shear modulus, while the exponent is 3.4-3.7 for the viscosity.[52] However, interestingly one observes that this increase of the more viscosity-like quasi-property η_α, becomes much less pronounced for the highest M_w of 4000 kDa. Apparently for this very long polymer chain the system is largely dominated already at lower concentrations by the elastic properties and therefore the concentration dependent increase of energy dissipation becomes less pronounced.

Table 2: Power-law scaling exponents of the quasi-properties η_α and η_β with concentration.

M_w	n_α	n_β
1000 kDa	4.66	2.95
2000 kDa	4.86	3.17
4000 kDa	3.09	3.07

The corresponding fractional exponents, α and β, are shown in Figure 5 B). For lower viscous samples, such as 4000 kDa 1 wt% and 2000 kDa/1000 kDa 2 wt%, one finds $\alpha = 1$, meaning the spring-pot is a regular dashpot and the quasi-properties

are regular viscosities. However, β is not zero but in the range of 0.5 to 0.1, decreasing systematically with increasing M_w of the PEO chains. This means that the elastic properties of the system depend substantially on the length of the polymer chain. With increasing polymer concentration, α and β both decrease, meaning that the systems behaves more elastically and the corresponding quasi-properties are more modulus-like. Looking more closely at Figure 5 B), it is evident that the difference α-β does not change strongly with concentration but remains rather constant at around 0.5-0.6, which is an interesting finding that indicates that for this fractional model both spring-pots change their properties in a systematic and similar way.

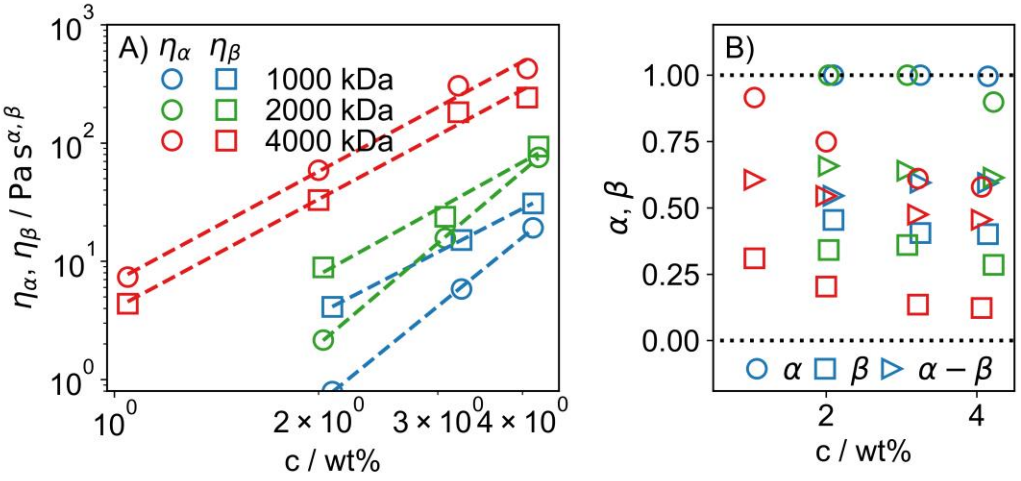

Figure 5: Variation of fit parameters with polymer concentration. A) The quasi-properties η_α and η_β show power scaling as indicated by the broken lines. B) Fractional exponents α and β decrease with concentration while their difference α-β remains relatively unchanged (color code is the same as in 5A; blue: 1000 kDa, green: 2000 kDa, red: 4000 kDa).

5. Conclusion

We have shown that the fractional Maxwell model (FMM) yields an excellent description of the frequency-dependent rheology of PEO solutions with fewer model parameters compared to the classical, generalized Maxwell model (GMM). The GMM's prediction becomes unreliable beyond the experimental fit range, whereas the FMM provides a reasonable prediction, indicating that its model parameters fully capture the sample rheology. The zero-shear viscosity of the FMM diverges, contrary to what is found experimentally, meaning that it is only valid in a finite, albeit large, time or frequency range. We have derived an analytical expression for the relaxation time spectrum $H(\tau)$ as a function of the FMM parameters, bridging the gap between

the two modeling frameworks. The spectrum is given by two power-laws with exponents α and β. This analytical expression is mathematically equivalent to empirical expressions found in the literature. The predicted relaxation time spectra compare well to those obtained by applying the parsimonious model. The quasi-properties η_α and η_β shift the respective power-law up and down, acting on infinitely many relaxation modes simultaneously. η_α and η_β themselves show power-law scaling as a function of polymer concentration, similar to regular viscosities and moduli. At the same time, the exponents α and β are becoming systematically smaller with increasing concentration and M_w of PEO, indicating the increasing elastic character of the solutions. Our findings provide a physical interpretation for the parameters of fractional viscoelastic models by associating them with more tangible relaxation time spectra. This allows to combine the advantages of both fractional and classical models. Similar analytic expressions for the spectra could be derived for other fractional viscoelastic models and should allow to gain a more advanced understanding of different types of hydrogels, as they are of key importance to many practical situations in technical formations or the in world of biology.

ASSOCIATED CONTENT

Supporting Information

The supporting Information is attached as a separate file with the following contents:

Amplitude sweeps; Frequency sweeps including all FMM fits; Steady-shear experiments

AUTHOR INFORMATION

Corresponding Author

*E-mail: r.schmidt.1@tu-berlin.de

michael.gradzielski@tu-berlin.de

Author Contributions

Conceptualization: MG, RS and HW. Data Curation: RS. Formal Analysis: RS and HW. Investigation: RS. Writing/Original Draft Preparation: RS, HW, MG. Writing/Review & Editing: RS, HW and MG.

Data Availability

The data that supports the findings of this study are available from the corresponding author upon reasonable request.

Conflict of Interest

The authors declare no competing financial interest.

ACKNOWLEDGEMENTS

This study was funded by the Deutsche Forschungsgemeinschaft (DFG, German Research Foundation, Project ID 431232613) - SFB 1449 project A02. We acknowledge the support by the German Research Foundation. Further, RS would like to acknowledge the *Fonds der chemischen Industrie* for financial support.

ABBREVIATIONS

PEO, poly(ethylene oxide); FMM, fractional Maxwell model; GMM, generalized Maxwell model; MLF, Mittag-Leffler function

REFERENCES

(1) Tschoegl, N. W. *The Phenomenological Theory of Linear Viscoelastic Behavior: An Introduction*; Springer Science & Business Media, 2012.

(2) Bonfanti, A.; Kaplan, J. L.; Charras, G.; Kabla, A. Fractional Viscoelastic Models for Power-Law Materials. *Soft Matter* **2020**, *16* (26), 6002–6020. https://doi.org/10.1039/D0SM00354A.

(3) Aime, S.; Cipelletti, L.; Ramos, L. Power-law Viscoelasticity of a Fractal Colloidal Gel. *J Rheol* **2018**, *62* (6), 1429–1441. https://doi.org/10.1122/1.5025622.

(4) Patrício, P.; Leal, C. R.; Duarte, J.; Januário, C. Rheology of the Cytoskeleton as a Fractal Network. *Phys Rev E Stat Nonlin Soft Matter Phys* **2015**, *92* (4), 040702. https://doi.org/10.1103/PHYSREVE.92.040702/FIGURES/3/MEDIUM.

(5) Dahesh, M.; Banc, A.; Duri, A.; Morel, M. H.; Ramos, L. Spontaneous Gelation of Wheat Gluten Proteins in a Food Grade Solvent. *Food Hydrocoll* **2016**, *52*, 1–10. https://doi.org/10.1016/J.FOODHYD.2015.06.014.

(6) Takenaka, M.; Kobayashi, T.; Saijo, K.; Tanaka, H.; Iwase, N.; Hashimoto, T.; Takahashi, M. Comparison in Fractal Dimension between Those Obtained from Structure Factor and Viscoelasticity of Gel Networks of 1,3:2,4-Bis-O-(p-Methylbenzylidene)-D-Sorbitol in Polystyrene Melt at Gel Point. *J Chem Phys* **2004**, *121* (7), 3323–3328. https://doi.org/10.1063/1.1770590.

(7) Matsumoto, T.; Kawai, M.; Masuda, T. Viscoelastic and SAXS Investigation of Fractal Structure near the Gel Point in Alginate Aqueous Systems. *Macromolecules* **1992**, *25* (20), 5430–5433. https://doi.org/10.1021/ma00046a047.

(8) Rubinstein, M.; Colby, R. H. *Polymer Physics*; Oxford University Press: London, England, 2003.

(9) Hang, J. T.; Kang, Y.; Xu, G. K.; Gao, H. A Hierarchical Cellular Structural Model to Unravel the Universal Power-Law Rheological Behavior of Living Cells. *Nature Communications 2021 12:1* **2021**, *12* (1), 1–7. https://doi.org/10.1038/s41467-021-26283-y.

(10) Djordjević, V. D.; Jarić, J.; Fabry, B.; Fredberg, J. J.; Stamenović, D. Fractional Derivatives Embody Essential Features of Cell Rheological Behavior. *Ann Biomed Eng* **2003**, *31* (6), 692–699. https://doi.org/10.1114/1.1574026/METRICS.

(11) Kohandel, M.; Sivaloganathan, S.; Tenti, G.; Darvish, K. Frequency Dependence of Complex Moduli of Brain Tissue Using a Fractional Zener Model. *Phys Med Biol* **2005**, *50* (12), 2799. https://doi.org/10.1088/0031-9155/50/12/005.

(12) Gobeaux, F.; Belamie, E.; Mosser, G.; Davidson, P.; Asnacios, S. Power-law Rheology and Strain-Induced Yielding in Acidic Solutions of Type I-Collagen. *Soft Matter* **2010**, *6* (16), 3769–3777. https://doi.org/10.1039/B922151D.

(13) Ng, T. S. K.; McKinley, G. H. Power-law Gels at Finite Strains: The Nonlinear Rheology of Gluten Gels. *J Rheol* **2008**, *52* (2), 417–449. https://doi.org/10.1122/1.2828018.

(14) Faber, T. J.; Jaishankar, A.; McKinley, G. H. Describing the Firmness, Springiness and Rubberiness of Food Gels Using Fractional Calculus. Part II: Measurements on Semi-Hard Cheese. *Food Hydrocoll* **2017**, *62*, 325–339. https://doi.org/10.1016/J.FOODHYD.2016.06.038.

(15) Laurent, V. M.; Fodil, R.; Cañadas, P.; Féréol, S.; Louis, B.; Planus, E.; Isabey, D. Partitioning of Cortical and Deep Cytoskeleton Responses from Transient Magnetic Bead Twisting. *Ann Biomed Eng* **2003**, *31* (10), 1263–1278. https://doi.org/10.1114/1.1616932/METRICS.

(16) Balland, M.; Desprat, N.; Icard, D.; Féréol, S.; Asnacios, A.; Browaeys, J.; Hénon, S.; Gallet, F. Power-laws in Microrheology Experiments on Living Cells: Comparative Analysis and Modeling. *Phys Rev E Stat Nonlin Soft Matter Phys* **2006**, *74* (2), 021911. https://doi.org/10.1103/PHYSREVE.74.021911/FIGURES/14/MEDIUM.

(17) Baumgaertel, M.; Winter, H. H. Determination of Discrete Relaxation and Retardation Time Spectra from Dynamic Mechanical Data. *Rheol Acta* **1989**, *28* (6), 511–519. https://doi.org/10.1007/BF01332922.

(18) Hilfer, R. *Applications of Fractional Calculus in Physics*; World scientific, 2000.

(19) Adolfsson, K.; Enelund, M.; Olsson, P. On the Fractional Order Model of Viscoelasticity. *Mech Time Depend Mater* **2005**, *9* (1), 15–34. https://doi.org/10.1007/s11043-005-3442-1.

(20) Jaishankar, A.; McKinley, G. H. A Fractional K-BKZ Constitutive Formulation for Describing the Nonlinear Rheology of Multiscale Complex Fluids. *J Rheol (N Y N Y)* **2014**, *58* (6), 1751–1788. https://doi.org/10.1122/1.4892114.

(21) Ki-Won, S.; Hoa-Youn, K.; Gap-Shik, C. Rheology of Concentrated Xanthan Gum Solutions: Oscillatory Shear Flow Behavior. *Korea-Australia Rheology Journal* **2006**, *18* (2), 67–81.

(22) Rosalina, I.; Bhattacharya, M. Dynamic Rheological Measurements and Analysis of Starch Gels. *Carbohydr Polym* **2002**, *48* (2), 191–202. https://doi.org/10.1016/S0144-8617(01)00235-1.

(23) Raee, E.; Avid, A.; Kaffashi, B. Effect of Compatibilizer Concentration on Dynamic Rheological Behavior and Morphology of Thermoplastic Starch/Polypropylene Blends. *J Appl Polym Sci* **2020**, *137* (22), 48742. https://doi.org/10.1002/app.48742.

(24) Wagner, C. E.; Barbati, A. C.; Engmann, J.; Burbidge, A. S.; McKinley, G. H. Quantifying the Consistency and Rheology of Liquid Foods Using Fractional Calculus. *Food Hydrocoll* **2017**, *69*, 242–254. https://doi.org/10.1016/j.foodhyd.2017.01.036.

(25) Abidine, Y.; Laurent, V. M.; Michel, R.; Duperray, A.; Palade, L. I.; Verdier, C. Physical Properties of Polyacrylamide Gels Probed by AFM and Rheology. *Europhys Lett* **2015**, *109* (3), 38003. https://doi.org/10.1209/0295-5075/109/38003.

(26) Caputo, M.; Mainardi, F. A New Dissipation Model Based on Memory Mechanism. *Pure Appl Geophys* **1971**, *91* (1), 134–147. https://doi.org/10.1007/BF00879562.

(27) Bagley, R. L.; Torvik, ; P J; Torvik, P. J. A Theoretical Basis for the Application of Fractional Calculus to Viscoelasticity. *J Rheol* **1983**, *27* (3), 201–210. https://doi.org/10.1122/1.549724.

(28) Koeller, R. C. Applications of Fractional Calculus to the Theory of Viscoelasticity. *J Appl Mech* **1984**, *51* (2), 299–307. https://doi.org/10.1115/1.3167616.

(29) Mainardi, F. *Fractional Calculus and Waves in Linear Viscoelasticity: An Introduction to Mathematical Models*; World Scientific, 2022.

(30) Rossikhin, Y. A.; Shitikova, M. V. Applications of Fractional Calculus to Dynamic Problems of Linear and Nonlinear Hereditary Mechanics of Solids. *Appl Mech Rev* **1997**, *50* (1), 15–67. https://doi.org/10.1115/1.3101682.

(31) Ramirez-Brewer, D.; Montoya, O. D.; Vivero, J. U.; García-Zapateiro, L. Characterization and Modeling of the Viscoelastic Behavior of Hydrocolloid-Based Films Using Classical and Fractional Rheological Models. *Fluids 2021, Vol. 6, Page 418* **2021**, *6* (11), 418. https://doi.org/10.3390/FLUIDS6110418.

(32) Jaishankar, A.; McKinley, G. H. Power-Law Rheology in the Bulk and at the Interface: Quasi-Properties and Fractional Constitutive Equations. *Proceedings of the Royal Society A: Mathematical, Physical and Engineering Sciences* **2013**, *469* (2149), 20120284. https://doi.org/10.1098/rspa.2012.0284.

(33) Miller, K. S.; Ross, B. *An Introduction to the Fractional Calculus and Fractional Differential Equations*; Wiley, 1993.

(34) Blair, G. W. S.; Coppen, F. M. v. The Subjective Conception of the Firmness of Soft Materials. *Am J Psychol* **1942**, *55* (2), 215–229. https://doi.org/10.2307/1417080.

(35) Yu, D. M.; Amidon, G. L.; Weiner, N. D.; Goldberg, A. H. Viscoelastic Properties of Poly(Ethylene Oxide) Solution. *J Pharm Sci* **1994**, *83* (10), 1443–1449. https://doi.org/10.1002/jps.2600831016.

(36) Ebagninin, K. W.; Benchabane, A.; Bekkour, K. Rheological Characterization of Poly(Ethylene Oxide) Solutions of Different Molecular Weights. *J Colloid Interface Sci* **2009**, *336* (1), 360–367. https://doi.org/10.1016/J.JCIS.2009.03.014.

(37) Rivero, D.; Gouveia, L. M.; Müller, A. J.; Sáez, A. E. Shear-Thickening Behavior of High Molecular Weight Poly(Ethylene Oxide) Solutions. *Rheol Acta* **2012**, *51* (1), 13–20. https://doi.org/10.1007/s00397-011-0569-7.

(38) Daga, V. K.; Wagner, N. J. Linear Viscoelastic Master Curves of Neat and Laponite-Filled Poly(Ethylene Oxide)–Water Solutions. *Rheol Acta* **2006**, *45* (6), 813–824. https://doi.org/10.1007/s00397-005-0059-x.

(39) Wiechert, E. Gesetze Der Elastischen Nachwirkung Für Constante Temperatur. *Ann Phys* **1893**, *286* (11), 546–570. https://doi.org/10.1002/andp.18932861110.

(40) Baumgaertel, M.; Winter, H. H. Interrelation between Continuous and Discrete Relaxation Time Spectra. *J Nonnewton Fluid Mech* **1992**, *44*, 15–36. https://doi.org/10.1016/0377-0257(92)80043-W.

(41) Ferry, J. D. *Viscoelastic Properties of Polymers*; John Wiley & Sons, 1980.

(42) Winter, H. H. Analysis of Dynamic Mechanical Data: Inversion into a Relaxation Time Spectrum and Consistency Check. *J Nonnewton Fluid Mech* **1997**, *68* (2), 225–239. https://doi.org/10.1016/S0377-0257(96)01512-1.

(43) Honerkamp, J.; Weese, J. Tikhonovs Regularization Method for Ill-Posed Problems. *Continuum Mechanics and Thermodynamics* **1990**, *2* (1), 17–30. https://doi.org/10.1007/BF01170953.

(44) Tschoegl, N. W.; Emri, I. Generating Line Spectra from Experimental Responses. Part II: Storage and Loss Functions. *Rheol Acta* **1993**, *32* (3), 322–327. https://doi.org/10.1007/BF00434196.

(45) Mead, D. W. Numerical Interconversion of Linear Viscoelastic Material Functions. *J Rheol (N Y N Y)* **1994**, *38* (6), 1769–1795. https://doi.org/10.1122/1.550526.

(46) Kamath, V. M.; Mackley, M. R. The Determination of Polymer Relaxation Moduli and Memory Functions Using Integral Transforms. *J Nonnewton Fluid Mech* **1989**, *32* (2), 119–144. https://doi.org/10.1016/0377-0257(89)85032-3.

(47) Honerkamp, J.; Weese, J. Determination of the Relaxation Spectrum by a Regularization Method. *Macromolecules* **1989**, *22* (11), 4372–4377. https://doi.org/10.1021/ma00201a036.

(48) Elster, C.; Honerkamp, J.; Weese, J. Using Regularization Methods for the Determination of Relaxation and Retardation Spectra of Polymeric Liquids. *Rheol Acta* **1992**, *31* (2), 161–174. https://doi.org/10.1007/BF00373238.

(49) Tschoegl, N. W.; Emri, I. Generating Line Spectra from Experimental Responses. III. Interconversion between Relaxation and Retardation Behavior. *International Journal of Polymeric Materials and Polymeric Biomaterials* **1992**, *18* (1–2), 117–127. https://doi.org/10.1080/00914039208034818.

(50) Friedrich, Chr.; Braun, H.; Weese, J. Determination of Relaxation Time Spectra by Analytical Inversion Using a Linear Viscoelastic Model with Fractional Derivatives. *Polym Eng Sci* **1995**, *35* (21), 1661–1669. https://doi.org/10.1002/pen.760352102.

(51) McDougall, I.; Orbey, N.; Dealy, J. M. Inferring Meaningful Relaxation Spectra from Experimental Data. *J Rheol (N Y N Y)* **2014**, *58* (3), 779–797. https://doi.org/10.1122/1.4870967.

(52) Stadler, F. J.; Bailly, C. A New Method for the Calculation of Continuous Relaxation Spectra from Dynamic-Mechanical Data. *Rheol Acta* **2009**, *48* (1), 33–49. https://doi.org/10.1007/s00397-008-0303-2.

(53) Honerkamp, J.; Weese, J. A Nonlinear Regularization Method for the Calculation of Relaxation Spectra. *Rheol Acta* **1993**, *32* (1), 65–73. https://doi.org/10.1007/BF00396678.

(54) Baumgaertel, M.; Schausberger, A.; Winter, H. H. The Relaxation of Polymers with Linear Flexible Chains of Uniform Length. *Rheol Acta* **1990**, *29* (5), 400–408. https://doi.org/10.1007/BF01376790.

(55) Grindy, S. C.; Learsch, R.; Mozhdehi, D.; Cheng, J.; Barrett, D. G.; Guan, Z.; Messersmith, P. B.; Holten-Andersen, N. Control of Hierarchical Polymer Mechanics with Bioinspired Metal-Coordination Dynamics. *Nat Mater* **2015**, *14* (12), 1210–1216. https://doi.org/10.1038/nmat4401.

(56) Koziol, M. F.; Nguyen, P. L.; Gallo, S.; Olsen, B. D.; Seiffert, S. Hierarchy of Relaxation Times in Supramolecular Polymer Model Networks. *Physical Chemistry Chemical Physics* **2022**, *24* (8), 4859–4870. https://doi.org/10.1039/D1CP04213K.

(57) Schiessel, H.; Metzler, R.; Blumen, A.; Nonnenmacher, T. F. Generalized Viscoelastic Models: Their Fractional Equations with Solutions. *J Phys A Math Gen* **1995**, *28* (23), 6567. https://doi.org/10.1088/0305-4470/28/23/012.

(58) Scott Blair, G. W. The Role of Psychophysics in Rheology. *J Colloid Sci* **1947**, *2* (1), 21–32. https://doi.org/10.1016/0095-8522(47)90007-X.

(59) Gorenflo, R.; Mainardi, F. Fractional Calculus. In *Fractals and Fractional Calculus in Continuum Mechanics*; Carpinteri, A., Mainardi, F., Eds.; Springer Vienna: Vienna, 1997; pp 223–276. https://doi.org/10.1007/978-3-7091-2664-6_5.

(60) Blair, G. W. S.; Veinoglou, B. C.; Caffyn, J. E. Limitations of the Newtonian Time Scale in Relation to Non-Equilibrium Rheological States and a Theory of Quasi-Properties. *Proc R Soc Lond A Math Phys Sci* **1947**, *189* (1016), 69–87. https://doi.org/10.1098/RSPA.1947.0029.

(61) Wu, F.; Liu, J. F.; Wang, J. An Improved Maxwell Creep Model for Rock Based on Variable-Order Fractional Derivatives. *Environ Earth Sci* **2015**, *73* (11), 6965–6971. https://doi.org/10.1007/s12665-015-4137-9.

(62) Ding, X.; Zhang, G.; Zhao, B.; Wang, Y. Unexpected Viscoelastic Deformation of Tight Sandstone: Insights and Predictions from the Fractional Maxwell Model. *Sci Rep* **2017**, *7* (1), 11336. https://doi.org/10.1038/s41598-017-11618-x.

(63) Shen, J. J.; Li, C. G.; Wu, H. T.; Kalantari, M. Fractional Order Viscoelasticity in Characterization for Atrial Tissue. *Korea-Australia Rheology Journal* **2013**, *25* (2), 87–93. https://doi.org/10.1007/s13367-013-0009-6.

(64) Holder, A. J.; Badiei, N.; Hawkins, K.; Wright, C.; Williams, P. R.; Curtis, D. J. Control of Collagen Gel Mechanical Properties through Manipulation of Gelation Conditions near the Sol–Gel Transition. *Soft Matter* **2018**, *14* (4), 574–580. https://doi.org/10.1039/C7SM01933E.

(65) Schmidt, R. F.; Kiefer, H.; Dalgliesh, R.; Gradzielski, M.; Netz, R. R. Nanoscopic Interfacial Hydrogel Viscoelasticity Revealed from Comparison of Macroscopic and Microscopic Rheology. *arXiv preprint arXiv:2312.07229* **2023**.

(66) Newville, M.; Stensitzki, T.; Allen, D. B.; Ingargiola, A. Lmfit: Non-Linear Least-Square Minimization and Curve-Fitting for Python. **2014**. https://doi.org/10.5281/ZENODO.1699739.

(67) Winter, H. H.; Mours, M. The Cyber Infrastructure Initiative for Rheology. *Rheol Acta* **2006**, *45* (4), 331–338. https://doi.org/10.1007/s00397-005-0041-7.

(68) Poh, L.; Narimissa, E.; Wagner, M. H.; Winter, H. H. Interactive Shear and Extensional Rheology—25 Years of IRIS Software. *Rheol Acta* **2022**, *61* (4), 259–269. https://doi.org/10.1007/s00397-022-01331-6.

(69) Wang, J.; Zhou, Y.; O'Regan, D. A Note on Asymptotic Behaviour of Mittag–Leffler Functions. *Integral Transform Spec Funct* **2018**, *29* (2), 81–94. https://doi.org/10.1080/10652469.2017.1399373.

(70) Özarslan, M. A.; Yılmaz, B. The Extended Mittag-Leffler Function and Its Properties. *J Inequal Appl* **2014**, *2014* (1), 85. https://doi.org/10.1186/1029-242X-2014-85.

(71) Haubold, H. J.; Mathai, A. M.; Saxena, R. K. Mittag-Leffler Functions and Their Applications. *J Appl Math* **2011**, *2011*, 298628. https://doi.org/10.1155/2011/298628.

(72) Garrappa, R. The Mittag-Leffler Function. MATLAB Central File Exchange October 13, 2015.

(73) Garrappa, R. Numerical Evaluation of Two and Three Parameter Mittag-Leffler Functions. *SIAM J Numer Anal* **2015**, *53* (3), 1350–1369. https://doi.org/10.1137/140971191.

(74) Ferry, J. D. *Viscoelastic Properties of Polymers*; Wiley, 1980.

(75) Chambon, F.; Winter, H. H. Stopping of Crosslinking Reaction in a PDMS Polymer at the Gel Point. *Polymer Bulletin* **1985**, *13* (6), 499–503. https://doi.org/10.1007/BF00263470.

(76) Winter, H. H.; Chambon, F. Rheology of Crosslinking Polymers at the Gel Point. In *Proc Bi-annual Meeting Polymer Networks Group, Elsinore*; 1986.

(77) Winter, H. H.; Chambon, F. Analysis of Linear Viscoelasticity of a Crosslinking Polymer at the Gel Point. *J Rheol (N Y N Y)* **1986**, *30* (2), 367–382. https://doi.org/10.1122/1.549853.

(78) Khandavalli, S.; Park, J. H.; Winter, H. H.; Myers, D. J.; Ulsh, M.; Mauger, S. A. Viscoelasticity Enhancement and Shear Thickening of Perfluorinated Sulfonic Acid Ionomer Dispersions in Water–Alcohol Solvent Mixtures. *Macromolecules* **2023**, *56* (17), 6988–7005. https://doi.org/10.1021/acs.macromol.3c00383.